Rock Mech Rock Eng (2017) 50:1205–1215
DOI 10.1007/s00603-016-1158-y

ORIGINAL PAPER

Modeling of Rock Joints Under Cyclic Loading Conditions Using Discontinuous Deformation Analysis

Shuqi Ma[1,2] · Chuan He[1] · Zhiye Zhao[2] · Wen Nie[2] · Xing Zhu[3] · Zhenyu Zhang[4]

Received: 8 March 2016 / Accepted: 27 December 2016 / Published online: 20 January 2017

Abstract The shear strength of rock joints is an important factor to be considered when analyzing the stability of jointed rock mass. Rock joints tend to have smaller shear resistances in the reverse shearing than that of the forward shearing. A conceptual model describing the general shear behavior of rock joints under cyclic loading and the Barton–Bandis joint model considering the surface roughness degradation are implemented into the two-dimensional discontinuous deformation analysis (DDA) model. The modified DDA model is empirically validated by cyclic shear tests on two types of rock joints. Numerical simulations agree well with the experimental results, indicating that the DDA model is capable of describing the varying shear behaviors of rock joints subjected to cyclic loading conditions.

Keywords Cyclic loading · Surface roughness degradation · Barton–Bandis joint model · DDA · Reverse shearing

✉ Zhiye Zhao
czzhao@ntu.edu.sg

[1] Key Laboratory of Transportation Tunnel Engineering, Ministry of Education, School of Civil Engineering, Southwest Jiaotong University, Chengdu 610031, People's Republic of China

[2] School of Civil and Environmental Engineering, Nanyang Technological University, Singapore 639789, Singapore

[3] State Key Laboratory of Geohazard Prevention and Geoenvironment Protection, Chengdu University of Technology, Chengdu 610059, People's Republic of China

[4] State Key Laboratory of Coal Mine Disaster Dynamics and Control, Chongqing University, Chongqing 400044, People's Republic of China

List of symbols

R_n	Normal component of the contact force
k_n	Stiffness of the normal springs
d_n	Penetration in normal direction
R_s	Shear component of the contact force
k_s	Stiffness of the shear springs
d_s	Relative shear displacement of the contact
$\emptyset$	Joint friction angle
c	Cohesion per unit length
l_c	Computed length of the contact
σ_n	Normal stress acting on the joint
$\emptyset_r$	Residual friction angle
$\emptyset_b$	Base friction angle
M	Damage parameter
$R_{s,peak}$	Peak shear force of the angle-edge contact
$d_{s,peak}$	Shear displacement required to reach the peak shear strength $R_{s,peak}$

Abbreviations

DDA	Discontinuous deformation analysis
JRC	Joint roughness coefficient
JCS	Joint compressive strength
JRC_{mob}	Mobilized joint roughness
JRC_{peak}	Peak JRC value before degradation

1 Introduction

Many studies have been carried out on rock joints under monotonic loading (Tang et al. 2014; Xia et al. 2014; Fathi et al. 2016) and under cyclic loading (Plesha 1987; Hutson and Dowding 1990; Huang et al. 1993; Jing et al. 1993; Lee et al. 2001). For rock joints under cyclic loading, joints will dilate in forward shearing and contract in the reverse

shearing in the normal direction, due to the presence of asperities on the joint surface. The term forward shearing refers to that the joint is sheared away from its original position, whereas the term reverse shearing means that the joint is moved toward its original position. One noticeable feature of the shear stress versus shear displacement curve of rock joints under cyclic loading is the smaller shear stress for the reverse shearing than that of the forward shearing. Reversal of the shear direction could be caused by earthquakes, blasting, rock bursts, and thermal loads (Ghosh et al. 1995). Failure to account for the decreased joint shear strength for the reverse shearing will overestimate the stability of fractured rock mass.

Discontinuous deformation analysis (DDA) is a numerical analysis method proposed by Shi (1988) to model the behavior of discontinuous medium. It takes into account the deformation of individual blocks as well as the interaction of blocks along discontinuities. Discontinuous blocky systems in DDA are formed by assembling discrete blocks together, and the motions of contacting blocks are governed by stiff springs. A dual form of DDA is developed by Zheng et al. (2016) where the contact forces rather than the displacements are used as the basic variables and contact springs are not involved.

Rock joints can significantly influence the strength of jointed rock mass. Mohr–Coulomb criterion is used in DDA to control the shearing movements between contacting blocks. When joints are subjected to compressive loading, the contacting blocks are initially 'locked' in the shearing direction until the generated inter-block shear forces of the joint contact are larger than the peak shear strength defined by Mohr–Coulomb's law in DDA. In the state of 'sliding,' the shear springs would be removed from the contact positions and blocks are 'sliding' along the joint. The joint shear force is computed by Mohr–Coulomb's law where cohesion is completely removed and the friction angle is maintained the same. Improper removal of cohesion when the joint contact shifts from 'locked' to 'sliding' might lead to incorrect assessment of the stability of geotechnical structures (Zheng et al. 2013; Wang et al. 2013). In order to overcome these problems, Wang et al. (2013) suggested a displacement-dependent shear strength criterion in which cohesion and friction angle are decreased along with the relative movements between the contacting blocks. Interfacial shear strength degradation of rock joints has also been proposed to provide more realistic simulations in DDA (Sitar et al. 2005; Bakun-Mazor et al. 2012). Despite these studies on joint shear behavior in DDA, very few studies have been reported in the use of DDA for modeling rock joints subjected to cyclic loading where shear loading direction is repeatedly reversed.

A number of constitutive models have been proposed for shear behaviors of rock joints (Patton 1966; Ladanyi and Archambault 1969; Plesha 1987; Barton and Bandis 1982; Jing et al. 1993; Lee et al. 2001). Most of these models are developed for monotonic shear loading. Barton–Bandis' empirical model (Barton and Bandis 1982) has been widely used as it is easy to apply and adopts several important factors of joint properties. Plesha (1987) proposed a constitutive model for both monotonic and cyclic shear loading in the framework of the classical plastic theory, in which the asperity angle is mobilized as a function of the work dissipated by the frictional sliding. Lee et al. (2001) modified Plesha's model by considering the asperity angle as the sum of the first- and second-order asperity angles. Jing et al. (1993) presented a conceptual model to describe the general behaviors of rock joints under cyclic shear loading. Based on this conceptual model, Jing et al. (1993) proposed a constitutive model for rock joints subjected to both monotonic and cyclic shear loading.

Jing et al. (1993)'s conceptual model took into account the assumption that the rock joint will dilate in the forward shearing and will contract during the reverse shearing. It is worth noticing that this assumption is not always correct. For instance, when rock joint with a low strength is subjected to a high normal stress, the asperity plane might be completely sheared off during the forward shearing process in the first loading cycle, and hence, there may be no obvious dilation in the forward shearing. Rock joints would not contract during the reverse shearing. The shearing behavior of rock joints depends on not only the joint profile, but also the joint strength and the normal stress.

This study is based on the assumption that the rock joint will dilate in the forward shearing and will contract during reverse shearing. The Barton–Bandis joint model together with the conceptual model proposed by Jing et al. (1993) is implemented into the DDA code to predict the behaviors of rock joints under cyclic loading conditions.

2 Two-Dimensional Discontinuous Deformation Analysis Method

Shi (1988) proposed discontinuous deformation analysis (DDA) by minimizing the total potential energy of a discontinuous block system. Every block in DDA method has six basic variables which includes three rigid body motion terms and three constant strain terms. The displacement vector of block i can be expressed by:

$$\boldsymbol{D_i} = \left(u_0, v_0, r_0, \varepsilon_x, \varepsilon_y, \gamma_{xy}\right)^T \tag{1}$$

where (u_0, v_0) refers to the rigid block translation of a specific point (x_0, y_0) in the block, r_0 is the rotation angle of the block with respect to the point (x_0, y_0), ε_x and ε_y refer to the normal strain components in the x and y directions,

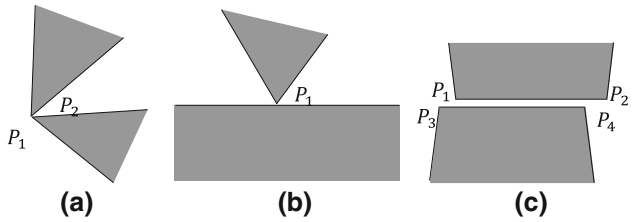

Fig. 1 Three possible contacts in 2D DDA: **a** angle-to-angle; **b** angle-to-edge; and **c** edge-to-edge

respectively, and γ_{xy} refers to the shear strain component. The displacement (u, v) of any point (x, y) in the block is:

$$\begin{Bmatrix} u \\ v \end{Bmatrix} = \begin{bmatrix} 1 & 0 & -(y-y_0) & (x-x_0) & 0 & (y-y_0)/2 \\ 0 & 1 & (x-x_0) & 0 & (y-y_0) & (x-x_0)/2 \end{bmatrix} \begin{Bmatrix} u_0 \\ v_0 \\ r_0 \\ \varepsilon_x \\ \varepsilon_y \\ \gamma_{xy} \end{Bmatrix} \quad (2)$$

The simultaneous equilibrium equations for a blocky system consisting of n blocks can be represented by:

$$\begin{bmatrix} K_{11} & K_{12} & \cdots & K_{1n} \\ K_{21} & K_{22} & \cdots & K_{2n} \\ \vdots & \vdots & \ddots & \vdots \\ K_{n1} & K_{n2} & \cdots & K_{nn} \end{bmatrix} \begin{bmatrix} D_1 \\ D_2 \\ \vdots \\ D_n \end{bmatrix} = \begin{bmatrix} F_1 \\ F_2 \\ \vdots \\ F_n \end{bmatrix}, \quad (3)$$

where K_{ii} is a 6×6 sub-matrix determined by the material parameters of block i, $K_{ij}(i \neq j)$ is a 6×6 sub-matrix representing the contacts between blocks i and j, D_i is a 6×1 sub-matrix representing the displacement vector of block i, and F_i is 6×1 sub-matrix representing the load vector of block i.

Once the block system deforms, the displacement vector D_i can be computed by solving the equilibrium equations. Based on the obtained results, the requirements of non-penetration and non-tension are checked. Very stiff springs will be added at the contacts in the normal direction in the occurrence of the block penetration or removed in the case of tension failure.

There are three possible types of contacts in two-dimensional (2D) DDA method, namely angle-to-angle contact, angle-to-edge contact, and edge-to-edge contact, as shown in Fig. 1. An edge-to-edge contact can be converted to two angle-to-edge contacts. For instance in Fig. 1c, the p_1p_2–p_3p_4 contact can be treated as angle p_1 to edge p_3p_4 contact and angle p_4 to edge p_1p_2 contact. There are three contact states in 2D DDA which are listed in Table 1. These contact states are governed by the penetration degrees and shear strength of the joint.

In Fig. 2, an edge-to-edge contact of length L subjected to normal compressive stress is converted into two angle-to-edge contacts of length l_c ($L = 2l_c$). Shear and normal

Table 1 Three contact states in 2D DDA

State	Normal component and shear component of the contact force	Remarks
Open	$R_n = -k_n d_n \leq 0$	The normal component of the contact force is tensile
Sliding	$R_n = -k_n d_n > 0$ and $R_s > R_n \tan \emptyset + cl_c$	The normal component of the contact force is compressive, and the mobilized shear force is larger than the maximum resisting shear force
Locked	$R_n = -k_n d_n > 0$ and $R_s = k_s d_s \leq R_n \tan \emptyset + cl_c$	The normal component of the contact force is compressive, and the mobilized shear force is less than or equal to the maximum resisting shear force

R_n is the normal component of the contact force; k_n is the stiffness of the normal springs; d_n is the penetration in normal direction; R_s is the shear component of the contact force; k_s is the stiffness of the shear springs; d_s is the relative shear displacement of the contact; $\emptyset$ is the joint friction angle; c is the cohesion per unit length; and l_c is the computed length of the contact

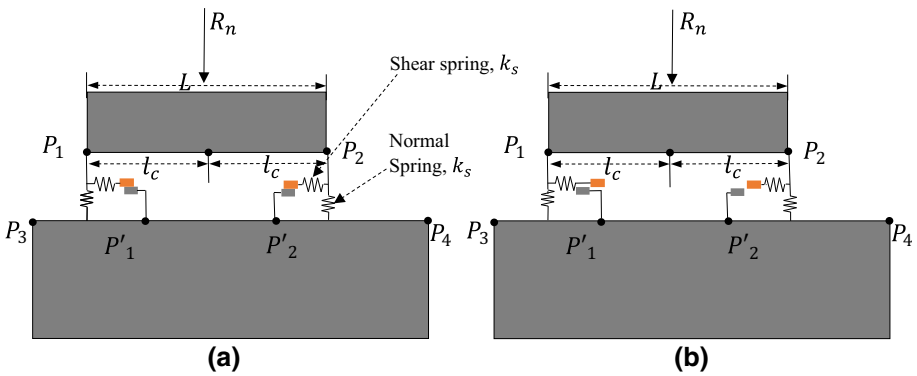

Fig. 2 An edge-to-edge contact **a** in state of 'locked' **b** in state of 'sliding'

springs of these two angle-to-edge contacts are conceptually illustrated in Fig. 2. P_1 and P_2 on the upper block are locked on P_1' and P_2', respectively, in the shear direction on edge P_3P_4. For an angle-to-edge contact, i.e., P_1-to-P_3P_4, the movement of P_1 relative to P_1' is controlled by a shear spring along the edge P_3P_4 according to the Mohr–Coulomb's law. The mobilized shear force of P_1-to-P_3P_4 is computed by $R_s = k_s d_s$. When the Mohr–Coulomb's law allows sliding ($R_s > R_n \tan \emptyset + cl_c$), the shear spring is removed from the contact and the shear strength of the contact is governed by the friction between the contacting blocks ($R_s = R_n \tan \emptyset$). Once the contact state changes from 'locked' to 'sliding,' cohesion is completely removed, while the friction angle is maintained the same.

In this paper, the displacement-dependent Barton–Bandis joint model is used for the shear failure evaluation of each contact. The Barton–Bandis joint model does not include cohesion, and its shear strength is characterized by the wall-roughness parameter JRC (joint roughness coefficient) and wall-strength parameter JCS (joint compressive strength).

3 Barton–Bandis Joint Model and Its Implementation in DDA

Based on the experimental shear tests, Barton (1973) presented a nonlinear shear strength criterion for rock joints.

$$\tau = \sigma_n \tan\left(\mathrm{JRC}\log_{10}\left(\frac{\mathrm{JCS}}{\sigma_n}\right) + \emptyset_r\right) \tag{4}$$

where: σ_n denotes the normal stress acting on the joint; $\emptyset_r$ denotes the residual friction angle, which equals to the base friction angle $\emptyset_b$ in the case of unweathered joint surfaces; JRC is the joint roughness coefficient; and JCS is the joint compressive strength.

Barton and Bandis (1982) recommended the use of mobilized roughness $\mathrm{JRC_{mob}}$ in Eq. (4), where the value of JRC is gradually decreased to account for asperity degradation during shear process. The ratio of $\mathrm{JRC_{mob}/JRC_{peak}}$ is a function of the ratio of current shear displacement to peak shear displacement, $d_s/d_{s,peak}$.

The peak shear force of the contact in DDA is controlled by Eq. (5) which is modified from Eq. (4).

$$R_{s,peak} = R_n \tan\left(\mathrm{JRC_{peak}}\log_{10}\left(\frac{\mathrm{JCS}}{\frac{R_n}{l_c}}\right) + \emptyset_r\right) \tag{5}$$

where l_c is the computed angle-edge contact length, which is half of the whole joint length; $R_{s,peak}$ is the peak shear force of the angle-edge contact; R_n is the normal force of the contact; and $\mathrm{JRC_{peak}}$ denotes the peak JRC value before degradation.

For joint contacts subjected to compressive loading, each angle-edge contact has two states: 'locked' and 'sliding.' In the case of $R_s \le R_{s,peak}$, i.e., the contact is 'locked,' the shear force of the contact is calculated by the shear spring stiffness and the relative shear displacement of the contact:

$$R_s = k_s d_s \tag{6}$$

The shear spring stiffness of joint contact k_s can be computed by

$$k_s = R_{s,peak}/d_{s,peak} \tag{7}$$

where $d_{s,peak}$ refers to the shear displacement required to reach the peak shear strength $R_{s,peak}$ of the contact.

When the developed shear force is larger than the peak shear strength ($R_s > R_{s,peak}$), the shear spring is removed from the contact position and the joint starts to slide. The shear force of the angle-to-edge contact will be computed by the Barton–Bandis model in which the displacement-dependent $\mathrm{JRC_{mob}}$ is used.

$$R_s = R_n \tan\left(\mathrm{JRC_{mob}}\log_{10}\left(\frac{\mathrm{JCS}}{\frac{R_n}{l_c}}\right) + \emptyset_r\right) \tag{8}$$

Barton (1982) proposed an equation to represent the mobilized tangent dilation angle d_t during the shear process.

$$d_t = \frac{1}{M}\mathrm{JRC_{mob}}\ \log_{10}\left(\frac{\mathrm{JCS}}{\sigma_n}\right) \tag{9}$$

where M is a damage parameter which equals to 1 and 2 under low and high normal stresses, respectively. When implementing Eq. (9) into DDA code, σ_n is replaced by $\frac{R_n}{l_c}$.

The dilation increment Δd_n can be computed by the shear displacement increment and the tangent dilation angle:

$$\Delta d_n = \Delta d_s \tan d_t. \tag{10}$$

4 Jing et al. (1993)'s Conceptual Model for Cyclic Loading and Its Implementation in DDA

Jing et al. (1993)'s conceptual model for rock joints under cyclic shear loading conditions and constant normal stress is modified and adopted in this study. Figure 3 shows the idealized shear behaviors of the conceptual model for rock joints under the first cycle and subsequent cycles. A complete shear cycle is divided into six different stages including three forward stages and three backward stages: forward advance stage (path $\overline{OABC}$); forward unloading stage (path $\overline{CD}$); forward return stage (path $\overline{DE}$); backward advance stage (path $\overline{EFGH}$); backward unloading stage (path $\overline{HI}$); and backward return stage (path $\overline{IJ}$).

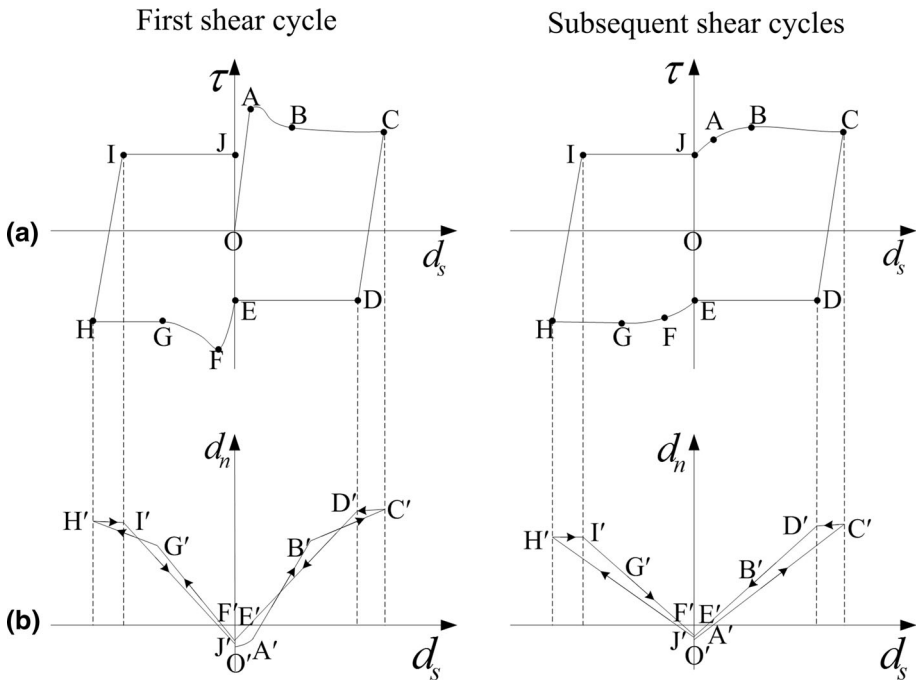

Fig. 3 A conceptual model for rock joints under cyclic loading and constant normal stress, modified from Jing et al. (1993). **a** Shear stress versus shear displacement curves; **b** dilation versus shear displacement curves

1. Forward advance stage (path $\overline{OABC}$)

Starting from the original point O, the shear stress increases linearly to the peak point A when the joint is sheared away from its original position. As the forward shear advances, the shear stress decreases to point B and reaches the residual shear stress at point C. In DDA, the joint contacts for the segment $\overline{OA}$ are in the state of 'locked.' The slope of $\overline{OA}$ is the joint shear stiffness k_s which is used together with Eq. (6) to calculate the shear forces for segment $\overline{OA}$. Once reaching the peak point B, the joint contacts start 'sliding' with the shear forces for $\overline{ABC}$ being computed by Eq. (8). JRC_{mob} is mobilized downwards along the shear displacement.

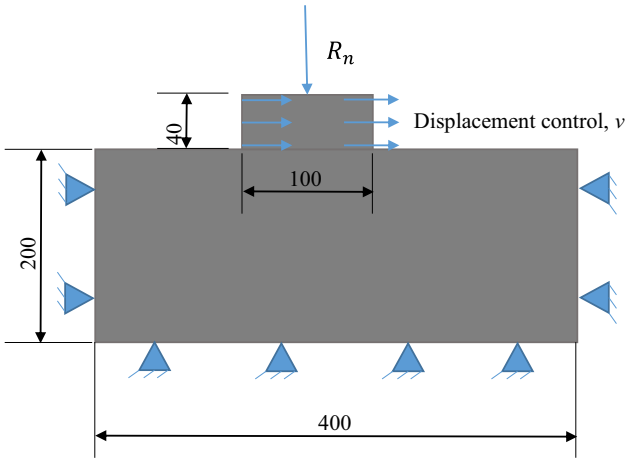

Fig. 4 Schematic sketch of DDA numerical model for cyclic shear test, in millimeters

The prominent peak shear stress shown in the shear stress versus shear displacement curve for the first shear cycle is disappeared in subsequent shear cycles where the joint contacts are maintained in the state of 'sliding.' Figure 3b shows the corresponding dilation path $\overline{O'A'B'C'}$ where the rate of dilation is gradually decreased.

2. Forward unloading stage (path $\overline{CD}$)

Upon the shear direction reversal at point C, the shear stress decreases proportionally along the shear displacement, which is represented by the segment $\overline{CD}$ in Fig. 3a. In the forward unloading stage, the shear stress decreases to zero and subsequently increases in the negative direction until point D. The segment $\overline{CD}$ has the same slope k_s as that of the segment $\overline{OA}$. For the dilation behavior shown in Fig. 3b, the rock joint contracts with a constant dilation rate, which is represented by the segment $\overline{C'D'}$.

In this stage, the contact state is switched from 'sliding' to 'locked' in DDA. Shear springs are added in the contact with the spring distance $d_{s,c}$ being computed by:

Table 2 Parameters of DDA numerical model

Parameters	Value
Normal penalty value, k_n (N/m)	5e11
Young's modulus (Pa)	5e9
Poisson's ratio	0.25
Dynamic control parameter	0
Time-step size (s)	0.001

Table 3 Parameters used in DDA simulations of Lee et al. (2001)

Rock type	JCS (MPa)	$\emptyset_r$ (°)	σ_n (MPa)	τ_p (MPa)	$d_{s,peak}$ (mm)	JRC_{peak}	R_n (N)	k_s (N/m)	M
Granite	151	34.6	1	1.92	1.25	12.8	1e5	7.68e7	1
Marble	72	38.3	0.5	1.13	0.3	12.9	5e4	1.88e8	1

$$d_{s,c} = \frac{R_{s,c}}{k_s} \tag{11}$$

where $R_{s,c}$ is the current shear force at point C which is inherited from the forward advance stage; $d_{s,c}$ is the corresponding spring distance at point C.

3. Forward return stage (path $\overline{DE}$):

The rock joint in the forward return stage shows smaller shear resistances in comparison with that of the forward advance stage. During this stage, joint is returned to its original position. At point D, the shear springs are removed and the joint contacts in DDA are changed to the state of 'sliding.' The shear forces for path $\overline{DE}$ are determined by Eq. (8). The mobilized dilation angle, represented by $JRC_{mob}\log_{10}\left(\frac{JCS}{\frac{R_n}{l_c}}\right)$ in Eq. (8), becomes negative value in this stage as the joint recovers and contracts in the reverse shearing.

For the dilation curves in this stage, the joint contracts continuously at a steeper slope [the segment $\overline{D'E'}$ in Fig. 3b] than that of the previous unloading path $\overline{C'D'}$.

4. Backward advance stage (path $\overline{EFGH}$), backward unloading stage (path $\overline{HI}$), and backward return stage (path $\overline{IJ}$)

When sheared in the negative direction from the original point, the joint will experience three backward stages (i.e., backward advance stage, backward unloading stage, and backward return stage). The joint shear behavior in these backward stages has similar characteristics as in forward stages except that the backward advance stage (path $\overline{EFGH}$) does not have the linear shear stress versus shear

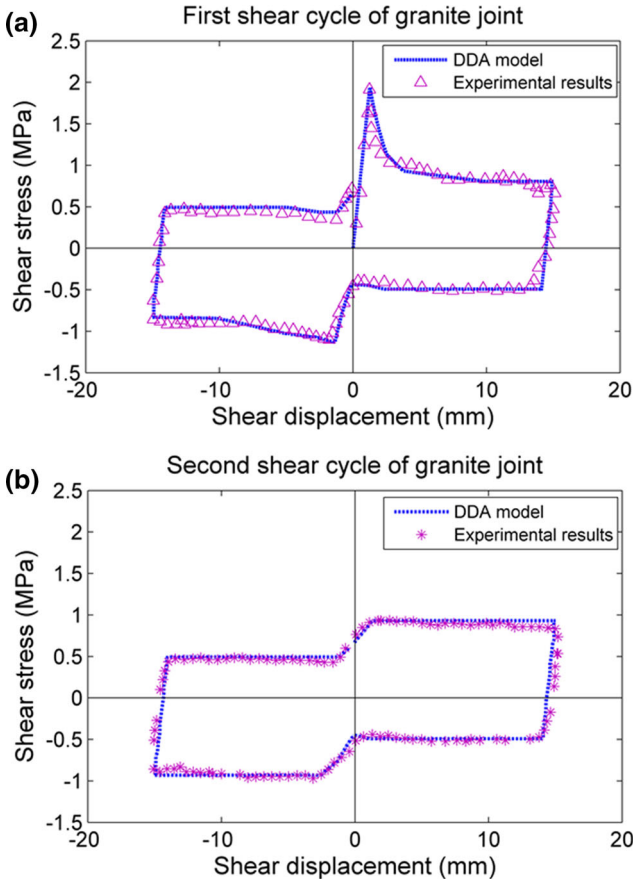

Fig. 5 Experimental and numerical shear stress versus shear displacement curves for the granite joint. **a** First shear cycle; **b** second shear cycle

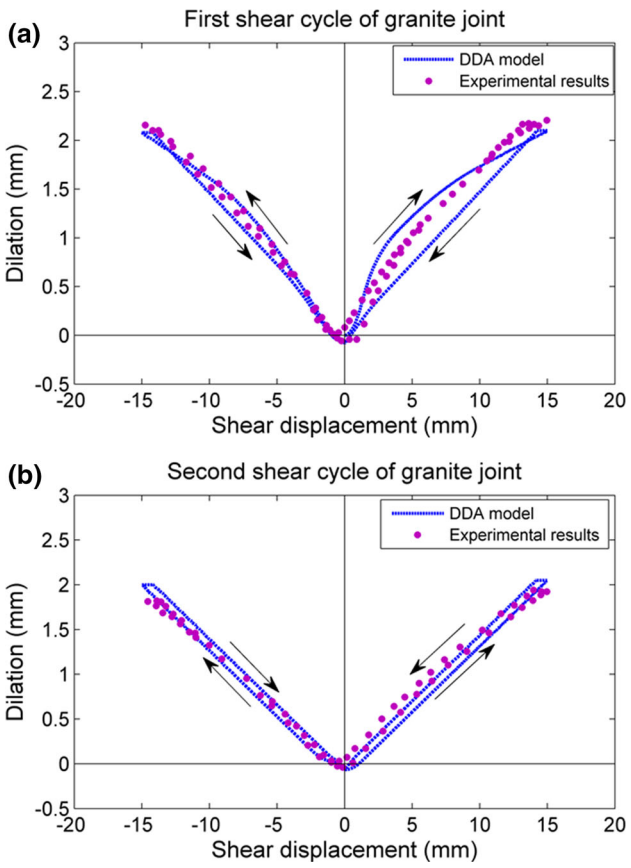

Fig. 6 Experimental and numerical dilation versus shear displacement curves for the granite joint. **a** First shear cycle; **b** second shear cycle

Table 4 Relationships of JRC_{mob}/JRC_{peak} and $d_s/d_{s,peak}$ for forward stages of the granite joint

$d_s/d_{s,peak}$	JRC_{mob}/JRC_{peak}			
	Forward advance stage of first cycle	Forward return stage of first cycle	Forward advance stage of second cycle	Forward return stage of second cycle
0	0	−0.4	0	−0.38
1	1	−0.38	0.3	−0.3
2	0.5	−0.3	0.3	−0.3
4	0.3	−0.3	0.3	−0.3
8	0.15	−0.3	0.3	−0.3
20	0.15	−0.3	0.3	−0.3

Table 5 Relationships of JRC_{mob}/JRC_{peak} and $d_s/d_{s,peak}$ for backward stages of the granite joint

$d_s/d_{s,peak}$	JRC_{mob}/JRC_{peak}			
	Backward advance stage of first cycle	Backward return stage of first cycle	Backward advance stage of second cycle	Backward return stage of second cycle
−20	0.15	−0.3	0.3	−0.3
−8	0.2	−0.3	0.3	−0.3
−4	0.4	−0.3	0.3	−0.3
−2	0.45	−0.4	0.3	−0.3
−1	0.5	−0.4	0.1	−0.3

displacement relationship as the forward advance stage. The shear forces for the backward unloading stage (path $\overline{HI}$) and backward return stage (path $\overline{IJ}$) can be calculated according to the details given for paths $\overline{CD}$ and $\overline{DE}$, respectively.

In the DDA modeling, Eq. (10) is used to calculate the joint dilation in the normal direction for all the shearing stages. The subsequent shear cycles shown in Fig. 3 have the similar shear behaviors as the first cycle except for the absence of the peak shear stress in the forward advance stages and backward advance stages. The shear forces for the subsequent cycles can be computed according to the procedures given for the first cycle. The asperity degradation during the shearing process is represented by the relationships of JRC_{mob}/JRC_{peak} and $d_s/d_{s,peak}$.

5 Validation of the Joint Model in DDA

A 2D DDA model consisting of two blocks as shown in Fig. 4 is employed for the numerical cyclic shear tests. The lower block is fixed in all directions. The normal force is applied in the middle of the upper block. After that, directional displacement constraint is applied on the upper block which is displaced at a constant velocity. The parameters used in these cyclic shear tests are listed in Table 2. Shi (1993) recommended that the normal penalty value k_n should be 10–100 times the elastic modulus of

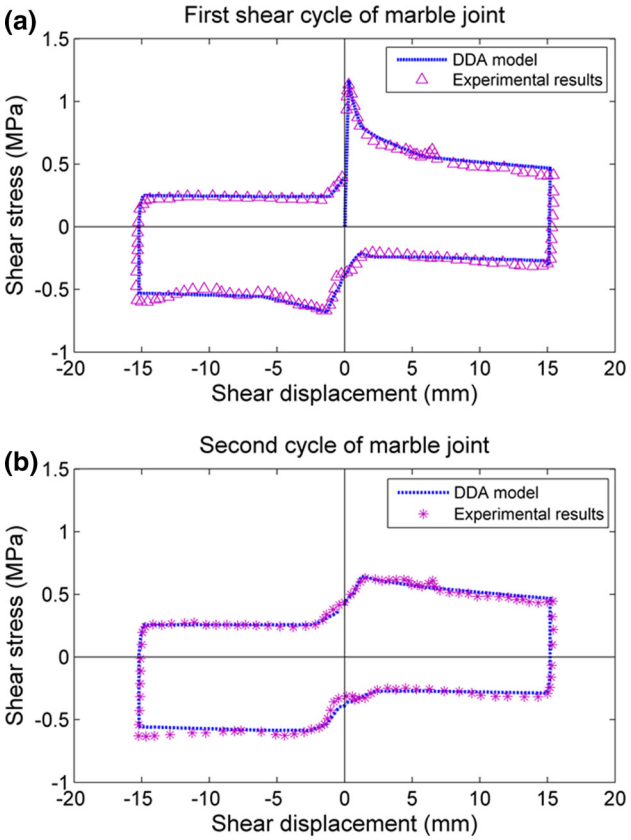

Fig. 7 Experimental and numerical shear stress versus shear displacement curves for the marble joint. **a** First shear cycle; **b** second shear cycle

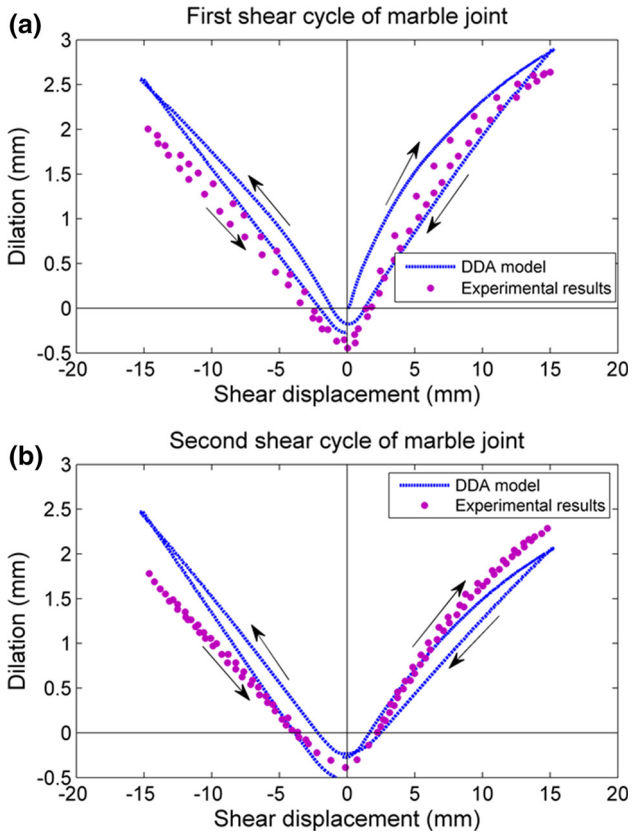

Fig. 8 Experimental and numerical dilation versus shear displacement curves for the marble joint. **a** First shear cycle; **b** second shear cycle

blocks in order to reach acceptable displacements and stresses.

Lee et al. (2001) conducted a series of cyclic shear tests on two types of rock joints (granite and marble joints) under constant stress. Two tests (granite joint under the normal stress of 1 MPa and marble joint under the normal stress of 0.5 MPa) were selected from Lee et al. (2001)'s study to verify the proposed model. The used parameters in the DDA simulations are listed in Table 3. JRC_{peak} value for peak point A was back-calculated based on the experimental results. The normal force R_n and shear spring stiffness k_s were calculated and are also given in Table 3. The remaining parameters in Table 3 were obtained based on Lee et al. (2001)'s experimental tests. The value of M in Eq. (9) for the two tests was 1 due to the low normal stresses applied on joints (0.5 and 1 MPa for the two tests, respectively).

5.1 Validation against Cyclic Shear Behaviors of Rough Granite Joint

The first two cycles of Lee et al. (2001)'s cyclic shear tests on rough granite joint subjected to the normal stress of 1 MPa was simulated by the DDA model. The obtained shear forces of the joint from the DDA simulation were converted to shear stresses. The shear stress versus shear displacement curves and the dilation versus shear displacement curves predicted by the DDA model are compared with those of experimental results as shown in Figs. 5 and 6, respectively. It can be seen that the proposed DDA model yields good predictions on the shear behaviors of rock joints for the first two consecutive cycles. The DDA model successfully reproduces the peak shear stress, the shear stress variation, dilation and contraction in advance, and unloading and return stages. The linear shear stress–shear displacement relationship caused by the shear direction reversal is also well represented by the DDA model.

The phenomenon of joint roughness degradation is governed by the relationships of JRC_{mob}/JRC_{peak} and $d_s/d_{s,peak}$, which are given in Tables 4 and 5. Table 4 is for forward stages and Table 5 is for backward stages. The relative shear displacement d_s for the joint contact is recorded in the DDA code. The current JRC value of the joint contact can then be obtained based on the computed

Table 6 Relationships of JRC_{mob}/JRC_{peak} and $d_s/d_{s,peak}$ for forward stages of the marble joint

$d_s/d_{s,peak}$	JRC_{mob}/JRC_{peak}			
	Forward advance stage of first cycle	Forward return stage of first cycle	Forward advance stage of second cycle	Forward return stage of second cycle
0	0	0	0.11	0
1	1	−0.1	0.2	−0.1
2	0.8	−0.3	0.25	−0.1
4	0.7	−0.55	0.5	−0.2
8	0.6	−0.45	0.45	−0.35
20	0.35	−0.45	0.35	−0.35
80	0	−0.26	0	−0.25

Table 7 Relationships of JRC_{mob}/JRC_{peak} and $d_s/d_{s,peak}$ for backward stages of the marble joint

$d_s/d_{s,peak}$	JRC_{mob}/JRC_{peak}			
	Backward advance stage of first cycle	Backward return stage of first cycle	Backward advance stage of second cycle	Backward return stage of second cycle
−80	0.25	−0.4	0.3	−0.45
−20	0.35	−0.4	0.4	−0.45
−8	0.5	−0.4	0.4	−0.4
−4	0.55	−0.4	0.3	−0.2
−2	0.3	−0.2	0.1	−0.1
−1	0.2	−0.1	0	−0.1

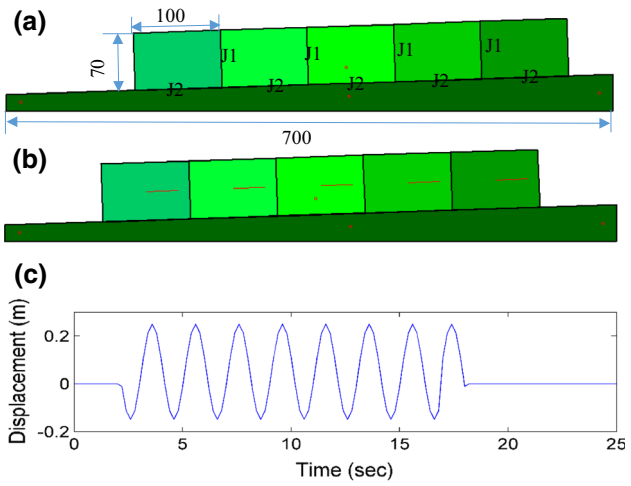

Fig. 9 Multi-block sliding modeling. **a** The model configuration before loading (unit: meter); **b** the configuration at the end of loading; **c** the input horizontal displacement time histories

Table 8 Parameters of DDA numerical model

Parameters	Value
Normal penalty value, k_n (N/m)	5e11
Shear penalty value, k_s (N/m)	3e7
Density (kg/m^3)	2000
Poisson's ratio	0.25
Dynamic control parameter	1
Time-step size (s)	0.005

d_s and the relationship of JRC_{mob}/JRC_{peak} and $d_s/d_{s,peak}$. The mobilized dilation angle represented by $JRC_{mob}\log_{10}\left(\frac{JCS}{\frac{\sigma_n}{l_c}}\right)$ is negative in the forward–backward return stages, which is consistent with the study of Lee et al. (2001).

5.2 Validation Against Cyclic Shear Behaviors of Rough Marble Joint

The first two cycles of Lee et al. (2001)'s cyclic shear tests on rough marble joint subjected to the normal stress of 0.5 MPa was also numerically modeled. Figures 7 and 8 show comparisons of numerical and experimental results for shear stress versus shear displacement curves and dilation versus shear displacement curves, respectively. Figure 7 shows that the predicted shear stresses match well with the measured shear stress of the experimental results for the two consecutive shear cycles. Despite the discrepancy between the predicted and measured dilation results as shown in Fig. 8, the DDA model still reproduces reasonable predictions of dilation behaviors for rough marble joints.

The relationships of JRC_{mob}/JRC_{peak} and $d_s/d_{s,peak}$ for the two consecutive shear cycles on marble joints are given in Tables 6 and 7. Table 6 is for forward stages and Table 7 backward stages. The mobilized dilation angle for marble joints' cyclic shear tests is also negative for return stages.

6 Blocks Sliding Under Horizontal Seismic Loading

A multiple-block system subjected to horizontal seismic loading is simulated to demonstrate the application of the modified DDA model. The sliding plane is inclined at an extremely small angle of 2°. This situation (the sliding angle of 2°) was encountered in a landslide triggered by the

Table 9 Parameters of joint materials

Joint materials	Frictional angle (°)	Cohesion (MPa)	Tensile strength (MPa)	$\emptyset_r$ (°)	$d_{s,peak}$ (m)	JRC_{peak}	JCS (MPa)
J1	20	0	10	NA	NA	NA	NA
J2	Equivalent of 8°	0	0	1	0.164	3.98	80

NA not applicable

Table 10 Relationships of JRC_{mob}/JRC_{peak} and $d_s/d_{s,peak}$ for the multi-blocking sliding

$d_s/d_{s,peak}$	−20	−8	−4	−2	−1	0	1	2	4	8	20
I	0.2	0.5	0.7	0.9	1	1	−1	−0.9	−0.7	−0.5	−0.2
II	$0.9^n \times 0.2$	$0.9^n \times 0.5$	$0.9^n \times 0.7$	$0.9^n \times 0.9$	$0.9^n \times 1$	$0.9^n \times 1$	$0.9^n \times (-1)$	$0.9^n \times (-0.9)$	$0.9^n \times (-0.7)$	$0.9^n \times (-0.5)$	$0.9^n \times (-0.2)$

I stands for "JRC_{mob}/JRC_{peak} in the initial shearing direction"; II is for "JRC_{mob}/JRC_{peak} in the nth shearing direction change"

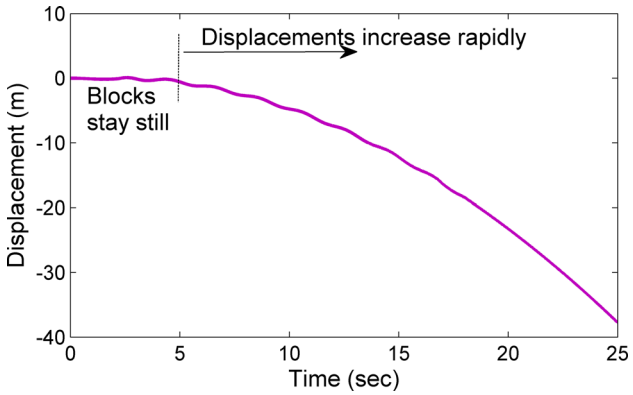

Fig. 10 The upper block relative sliding displacement to the base

2008 Iwate–Miyagi earthquake (Miyagi et al. 2011; Irie et al. 2009). The occurrence of the landslide with a very small sliding angle might be due to the reduction in the internal friction angle caused by the cyclic loading (Irie et al. 2009).

The configuration of the multi-block sliding model is illustrated in Fig. 9a. The parameters of the DDA model are listed in Table 8. Two joint materials J1 and J2 were used in the numerical simulation as shown in Fig. 9a. Joints between the upper blocks and the base block adopted the Barton–Bandis joint material, J2, while joints between the five upper blocks used the joint material J1. The parameters of the joint materials J1 and J2 are given in Table 9. The friction angle of J2 is equivalent to 8°. The shear resistance of joint J2 was decreased according to the relationship in Table 10. The degrading coefficients in the second row of Table 10 were simply mobilized down with the changes in the shear direction as shown in the third row of Table 10.

Ning and Zhao (2013) pointed out that applying the seismic accelerations as constraint displacement time histories to the base could produce the same results as the theoretical solutions. In the multi-block modeling, a horizontal constraint displacement time history shown in Fig. 9c was applied to the base block. The relative displacement of the third upper block to the base was measured during the modeling. The results are shown in Fig. 10. It can be seen that the upper blocks stayed almost still in the first 5 s. Afterward, the upper blocks started moving downward and the displacements increased rapidly, as the shearing resistance between the upper blocks and the base was reduced due to the cyclic loadings.

7 Conclusions

In the original DDA model, the Mohr–Coulomb's model often leads to an unrealistic prediction for shearing behaviors of rock joints under monotonic and cyclic shear

loadings. This paper makes an attempt to improve the DDA joint model so as to better capture the cyclic shearing behavior. Rock joints tend to have smaller shear strength during the reverse shearing phase than that in the forward shearing phase, and this phenomena impact on the real behavior of rock joints when subjected to drilling- and blasting-induced loads, and thermal and earthquake loads. The proposed model is able to represent the joint behaviors in both forward and reverse shearing movement, and the correct reverse shearing model can avoid overestimating the stability of slopes.

This paper provides a method to model the shear behaviors of rock joints under cyclic shear loading in 2D DDA. Jing et al. (1993)'s conceptual model combined with Barton–Bandis joint model was implemented into the DDA code. The shear stress versus the shear displacement curve for each shear cycle is divided into six different stages and discussed in detail. The phenomenon of asperity degradation is described by the relationships of JRC_{mob}/JRC_{peak} and $d_s/d_{s,peak}$. Once the shear direction is reversed, the joint contact is switched to the state of 'locked' with shear springs being added on the contact positions and the shear forces of the joint contacts are determined by the shear springs during unloading stages.

The proposed DDA joint model was validated by cyclic shear tests conducted by Lee et al. (2001). Comparisons between the DDA simulation and the experimental results indicate that the DDA joint model is capable of predicting the varying shear stress and dilation behaviors of rock joints under cyclic shear loading.

A multiple-block sliding model was carried out by applying a horizontal seismic loading to the base block. The interfacial shearing resistance was mobilized downwards due to the seismic loading. The upper blocks started sliding after 5 s of seismic loading, which explains the possibility of the occurrence of a landslide with a small sliding angle when subjected to an earthquake.

References

Bakun-Mazor D, Hatzor YH, Glaser SD (2012) Dynamic sliding of tetrahedral wedge: the role of interface friction. Int J Numer Anal Meth Geomech 36:327–343

Barton N (1973) Review of a new shear-strength criterion for rock joints. Eng Geol 7:287–332

Barton N (1982) Modelling rock joint behavior from in situ block tests: implications for nuclear waste respository design. Office of Nuclear Waste Isolation, Columbus, OH, 96 pp, ONWI-308

Barton N, Bandis S (1982) Effects of block size on the shear behaviour of jointed rock. Keynote lecture. In: 23rd US symposium on rock mechanics, Berkeley, California

Fathi A, Moradian Z, Rivard P, Ballivy G, Boyd AJ (2016) Geometric effect of asperities on shear mechanism of rock joints. Rock Mech Rock Eng 49:801–820. doi:10.1007/s00603-015-0799-6

Ghosh A, Hsiung SM, Chowdhury AH (1995) Seismic response of rock joints and jointed rock mass. Technical report, NUREG/CR-6388, CNWRA 95 013

Huang X, Haimson BC, Plesha ME, Qiu X (1993) An investigation of the mechanics of rock joints—part I. Laboratory investigation. Int J Rock Mech Min Sci Geomech Abstr 30:257–269

Hutson RW, Dowding CH (1990) Joint asperity degradation during cyclic shear. Int J Rock Mech Min Sci Geomech Abstr 27:109–119

Irie K, Koyama T, Hamasaki E, Nishiyama S, Shimaoka K, Ohnishi Y (2009) DDA simulations for huge landslides in Aratozawa Area, Miyagi, Janpan caused by Iwate-Miyagi Nairiku earthquake. In: Ma GW, Zhou YX (eds) Analysis of discontinuous deformation: new developments and applications. Research Publishing Services, Singapore, pp 153–160

Jing L, Stephansson O, Nordlund E (1993) Study of rock joints under cyclic loading conditions. Rock Mech Rock Eng 26:215–232

Ladanyi B, Archambault G (1969) Simulation of the shear behaviour of a jointed rock mass. In: The 11th symposium on rock mechanics, Berkeley, pp 105–125

Lee HS, Park YJ, Cho TF, You KH (2001) Influence of asperity degradation on the mechanical behavior of rough rock joints under cyclic shear loading. Int J Rock Mech Min Sci 38:967–980

Miyagi T, Yamashina S, Esaka F, Abe S (2011) Massive landslide triggered by 2008 Iwate–Miyagi inland earthquake in the Aratozawa Dam area, Tohoku, Japan. Landslides 8:99–108. doi:10.1007/s10346-010-0226-8

Ning Y, Zhao Z (2013) A detailed investigation of block dynamic sliding by the discontinuous deformation analysis. Int J Numer Anal Meth Geomech 37:2373–2393. doi:10.1002/nag.2140

Patton FD (1966) Multiple modes of shear failure in rock. In: Proceedings of the first congress ISRM, Lisbon, pp 509–513

Plesha ME (1987) Constitutive models for rock discontinuities with dilatancy and surface degradation. Int J Numer Anal Meth Geomech 11:345–362

Shi GH (1988) Discontinous deformation Analysis. PhD thesis, University of California, Berkeley, USA

Shi GH (1993) Block system modeling by discontinuous deformation analysis. Computational Mechanics Publications, Southampton

Sitar N, MacLaughlin M, Doolin D (2005) Influence of kinematics on landslide mobility and failure mode. J Geotech Geoenviron Eng 131:716–728

Tang Z, Liu Q, Xia C, Song Y, Huang J, Wang C (2014) Mechanical model for predicting closure behavior of rock joints under normal stress. Rock Mech Rock Eng 47:2287

Wang L, Jiang H, Yang Z, Xu Y, Zhu X (2013) Development of discontinuous deformation analysis with displacement-dependent interface shear strength. Comput Geotech 47:91–101

Xia C, Tang Z, Xiao W, Song Y (2014) New peak shear strength criterion of rock joints based on quantified surface. Descr Rock Mech Rock Eng 47:387–400. doi:10.1007/s00603-013-0395-6

Zheng L, Chen G, Zhang Y, Zhang H (2013) Review of rock stability analysis using discontinuous deformation analysis. In: Feng H, Tan (eds) Rock characterisation, modelling and engineering design methods. Taylor & Francis Group, London, pp 491–591

Zheng H, Zhang P, Du X (2016) Dual form of discontinuous deformation analysis. Comput Methods Appl Mech Eng 305:196–216. doi:10.1016/j.cma.2016.03.008